Food Chemistry: X 22 (2024) 101488

Contents lists available at ScienceDirect

Food Chemistry: X

journal homepage: www.sciencedirect.com/journal/food-chemistry-x

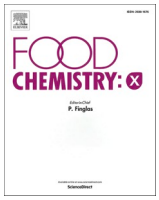

Development of an "on-off-on" fluoroprobe utilizing an anthrylimidazole-based fluorescent ionic liquid for sensitive Cr(VI) and ascorbic acid detection

He Mei [a,b], Ping Xu [c,1], Mengting Feng [a], Jianping Wang [a], Chenxin Zhang [c], Haibin Chen [a,b], Huili Wang [d], Junyi Guo [c,**], Xuedong Wang [d,**], Shugen Qu [a,b,*]

[a] Zhejiang Provincial Key Laboratory of Watershed Science and Health, College of Public Health, Wenzhou Medical University, Wenzhou 325035, China
[b] South Zhejiang Institute of Radiation Medicine and Nuclear Technology, Wenzhou 325809, China
[c] School and Hospital of Stomatology, Wenzhou Medical University, Wenzhou 325035, China
[d] School of Environmental Science and Engineering, Suzhou University of Science and Technology, Suzhou 215009, China

ARTICLE INFO

Keywords:
Anthrylimidazole-based fluorescent ionic liquid
"On-off-on" platform
Inner-filter effect
Photoinduced electron transfer
Cr(VI)
Ascorbic acid

ABSTRACT

Developing a rapid detection method of Cr(VI) and ascorbic acid (AA) is vital in the food and environmental fields. Herein, an anthrylimidazole-based fluorescent ionic liquid (AI-FIL) with the advantageous fluorescent properties was successfully prepared and used to construct a promising "on-off-on" fluoroprobe for rapid/sensitive Cr(VI) and AA detection. Cr(VI) could effectively quench the fluorescence of AI-FIL owing to the inner-filter effect and photoinduced electron-transfer process. However, the decreased fluorescence could be rapidly recovered by AA owing to the redox reaction between AA and Cr(VI). For Cr(VI) detection, a satisfactorily linear response (0.03–300 μM) was achieved with the corresponding detection limit of 9 nM. For AA detection, a good linearity from 1 to 1000 μM was obtained with the resultant detection limit of 0.3 μM. Moreover, the AI-FIL based fluoroprobe was successfully utilized for Cr(VI) and AA detection in food and water samples with satisfactory accuracy and precision.

1. Introduction

As an important kind of antioxidant, ascorbic acid (AA) widely exists in fresh fruits and vegetables (Yang et al., 2018). Also, AA is an essential vitamin involved in many metabolic processes, and its level is often related to several disorders, such as nerve defects and scurvy (Xu et al., 2019). Therefore, it is of great demand to detect AA to develop the food industry and maintain the health of the human body. Currently, some methods have been developed for the determination of AA, including electrochemistry (Jayaraman, Palani, RaoJonnalagadda, & Shanmugam, 2022), colorimetry (Guo et al., 2022), fluorometry (Wang et al., 2020), and chromatography (Chen, Jiang, & Sahayam, 2020).

Fluorometry has earned plentiful eyes due to its superiorities, such as high sensitivity, excellent selectivity, rapid detection, and easy operation. According to the previous reports, most of the fluorometry for directly detecting AA were designed based on "turn off" strategy owing to the quenching mechanism, such as inner filter effect (IFE), dynamic or static quenching effect, and aggregation-induced quenching effect (Alizadeh et al., 2020; Deng et al., 2023; Huang et al., 2022; Long et al., 2020). However, the fluorometry based on "turn off" strategy may cause false positive signals from other quenchers in real-world samples, which is less feasible for practical applications (Kim, Choi, & Kim, 2021). Moreover, it was demonstrated that the fluorometry in "turn on" strategy displayed better sensitivity and higher selectivity than that of "turn off" strategy (Gao, Xu, Hou, & Zhang, 2022). Therefore, it is highly desired to develop a novel fluorometry based on "turn-on" strategy to detect AA.

To the best of our knowledge, most of the fluorometry based on "turn-on" strategy for AA assay are dependent on the manganese dioxide nanosheets, cobalt oxy-hydroxide nanosheets, and ion (Fe^{3+}, Cr(VI),

* Corresponding author at: Zhejiang Provincial Key Laboratory of Watershed Science and Health, College of Public Health, Wenzhou Medical University, Wenzhou 325035, China.
** Co-corresponding authors.
E-mail addresses: gjy3479@163.com (J. Guo), zjuwxd@163.com (X. Wang), shugenju@wmu.edu.cn (S. Qu).
[1] He Mei and Ping Xu contributed equally to this work and shared the first authorship.

https://doi.org/10.1016/j.fochx.2024.101488
Received 25 January 2024; Received in revised form 6 May 2024; Accepted 17 May 2024
Available online 21 May 2024

Cu^{2+}, IO_4^-), which have been used as media. The fluorescence of fluoroprobe can be quenched by these medias and recovered with the addition of AA owing to the redox reaction between AA and these medias, which is referred to as an "on-off-on" strategy. However, the preparation process of manganese dioxide nanosheets and cobalt oxyhydroxide nanosheets are complex and time-consuming. Besides, the final reaction solution obtained after the detection of AA is harmful to the environment. Cr(VI) has raised great interest in heavy metal pollution due to its high toxicity, carcinogenesis, teratogenicity, and mutagenicity, even at trace levels (Chen et al., 2019; Zhang, Liu, Wu, Tao, & Li, 2020). Humans are often exposed to Cr(VI) through the food chain because many foods contain high concentrations of Cr (Chen et al., 2020; Kebede, Tilachew, Chirfa, & Gure, 2022). The accurate and rapid determination of Cr(VI) in foods is critical to evaluate their safety. As such, it is highly promising that the development of a novel fluorometry based on "turn on" strategy for AA assay utilizing Cr(VI) as a medium. The aforementioned idea can realize the role of "killing three birds with one stone", because it not only can be used to detect Cr(VI), but also detect AA with "turn on" strategy and remove Cr(VI) after AA assay.

So far, many fluoroprobes, including graphene quantum dots (GQDs), sulfur quantum dots (SQDs), silicon quantum dots (SiQDs), and carbon quantum dots (CQDs), have been developed to construct fluorometry for Cr(VI) and AA detection. Xiao's group utilized GQDs as viable fluoroprobes to construct a switch platform for sensitively detecting Cr (VI) and AA (Huang, Qiu, Zhu, Lu, & Xiao, 2015). Zhu and coworkers prepared water-dispersible fluorescent SiQDs with blue fluorescence, which was used to construct a fluorescence-switch platform for Cr(VI) and AA detection with high sensitivity (Xu et al., 2019). Zhou and Liu's teamwork synthesized carboxymethyl cellulose SQDs to establish an "on-off-on" fluorescent sensor for sensitively/selectively detecting Cr (VI)/AA (Duan et al., 2020). The fluorescence signals of these fluoroprobes are prominently decreased due to the IFE between the fluoroprobes and Cr(VI), while they are efficiently recovered upon the addition of AA owing to the fact that Cr(VI) is reduced to lower-valent Cr species, thus leading to eliminate the IFE (Duan et al., 2020; Huang et al., 2015; Xu et al., 2019). Although these nanomaterials used to construct fluoroprobes for Cr(VI) and AA detection display superior sensitivity, several drawbacks have greatly limited their practical applications (Zhang, Fang, Zhao, & Li, 2018; Tan, An, Pan, Liu, & Hu, 2021). These disadvantages include complexity, time consumption, and high temperature required for synthetic procedures, poor water solubility, low fluorescence stability, and serious toxicity of heavy metal-containing semiconductor quantum dots. Thus, it is of great urgency for the development of novel fluoroprobes with simple preparation procedures, green synthetic methods, as well as high biocompatibility.

Organic fluorophores with excellent fluorescent properties are often used to sensitively and selectively detect Cr(VI) and AA. As a type of the preferred organic salts, ionic liquids (ILs) confer many advantages, such as outstanding thermal stability, excellent dissolving capacity, and negligible vapor pressure. Therefore, ILs are widely employed as mobile phase additives or stationary phase in chromatography, sensitizing or quenching solvents in fluorescence analyses, and as "green" solvents in chemical synthesis owing to their environment-friendly feature (Greaves & Drummond, 2008). Fluorescent ionic liquids (FILs) are an exciting class of ILs, which are endowed with both the superior properties of fluorescent materials and ILs, and thus have been extensively used to construct fluorescent assay for its high fluorescence efficiency and tunable properties. Regretfully, the "on-off-on" fluorescent platforms based on FILs have rarely been reported. Thus, it is of great significance to develop a fluoroprobe based on the FILs with favorable characteristics for Cr(VI) and AA detection.

Inspired by the above research gap, we synthesized an anthrylimidazole-based FIL (AI-FIL) and rigorously analyzed its optical properties. The fluorescence intensities (FIs) of AI-FIL were gradually quenched with the increasing Cr(VI) concentrations. By virtue of the above phenomenon, a novel "on-off-on" fluoroprobe based on the AI-FIL was constructed for Cr(VI) detection with satisfactory sensitivity and selectivity. Because AA could reduce Cr(VI) to Cr(III), the FIs of AI-FIL were efficiently restored when AA was introduced into the AI-FIL/Cr (VI) mixed system, and thus AI-FIL could be further used to determine AA using Cr(VI) as a medium (See Scheme 1). As a result, the as-constructed hybrid system could be used to determine the concentrations of Cr(VI) and AA in environmental water and food samples, thereby exhibiting a great application potential in their conventional monitoring.

2. Experimental section

2.1. Reagents

The following analytical-grade reagents were purchased from Aladdin: AA, $CuSO_4 \bullet 5H_2O$, $Al(NO_3)_3 \bullet 9H_2O$, $CoCl_2 \bullet 6H_2O$, $CaCl_2$, Zn $(NO_3)_2 \bullet 6H_2O$, $MgCl_2$, NaCl, $AgNO_3$, $NiCl_2 \bullet 6H_2O$, $Fe_2(SO_4)_3 \bullet xH_2O$, $FeSO_4 \bullet 7H_2O$, $CrCl_3$ and $Na_3PO_4 \bullet 12H_2O$. The other reagents were procured from Sinopharm Chemical Reagent, including Na_2CO_3, dopamine, L-cysteine, L-tryptophan, glycine, sucrose, glucose, DL-serine, sodium citrate dihydrate, glutathione (GSH). *N*-trimethyl silylimidazole, 9-chloromethyl anthracene, tetrahydrofuran (THF), diethyl ether, $K_2Cr_2O_7$, $NaAc \bullet 3H_2O$, and HAc. Ultrapure water with electrical conductivity of $\geq$18.2 MΩ•cm was generated by a Milli-Q system (MA, USA) and used for preparing all work solutions.

2.2. Synthesis of the AI-FIL.

The AI-FIL, i.e., 1,3-bis (9-anthracenylmethyl) imidazolium chloride ([BAMIM]Cl), was fabricated according to Fu and coworkers' report with minor revisions (Fu, Meng, Lu, Fei, & Dyson, 2008). Briefly, *N*-trimethylsilyl imidazole (1.4 g) and 9-chloromethyl anthracene (4.5 g) were added into 50 mL of THF and dissolved under an inert atmosphere. Next, the mixed solution was placed into a thermostat water bath at 60 °C for 24 h. After the reaction, the resultant solution was filtrated and washed three times using diethyl ether. Finally, the solid powder was obtained by vacuum drying at 60 °C for 24 h.

2.3. Cr(VI) and AA detection.

In brief, 100 μL of the AI-FIL solution (0.01 mg/mL) and 800 μL of HAc-NaAc buffer (200 mM, pH 7.0) were homogeneously mixed under vortexing conditions. Subsequently, 100 μL of Cr(VI) at varying initial concentrations was added into the above mixed system. After a 5-min water-bath incubation, the fluorescent emission spectra were recorded in the range of 390–550 nm at the excitation wavelength of 370 nm.

For AA detection, 100 μL of the AI-FIL solution (0.01 mg/mL) was mixed with 700 μL of HAc-NaAc buffer (200 mM, pH 7.0). Next, the Cr (VI) solution (100 μL, 3 mM) was added to the mixture as mentioned above and incubated in a thermostat water bath for 5 min to form the AI-FIL/Cr(VI) homogenous solution by handshaking. Hereafter, the different concentrations of AA (100 μL) were mixed with the obtained AI-FIL/Cr(VI) homogeneous solution. Finally, after a 40-min water-bath incubation, the fluorescent detection was similar to the procedures described above for Cr(VI) detection.

2.4. Fluorescent detection of Cr(VI)/AA in environmental waters and foods.

To examine the actual applicability of the AI-FIL based fluoroprobe, environmental waters, and foods were selected as examples of real-world samples. For the environmental waters (river, lake, and tap waters) and commercial fruit juices (grape juice, lemon juice, and kiwi juice), the samples were firstly purified by 0.22-μm syringe filters to obtain their respective filtrates. According to China's industrial standard (SN/T 2210–2021), the rice samples, such as polished and brown rice,

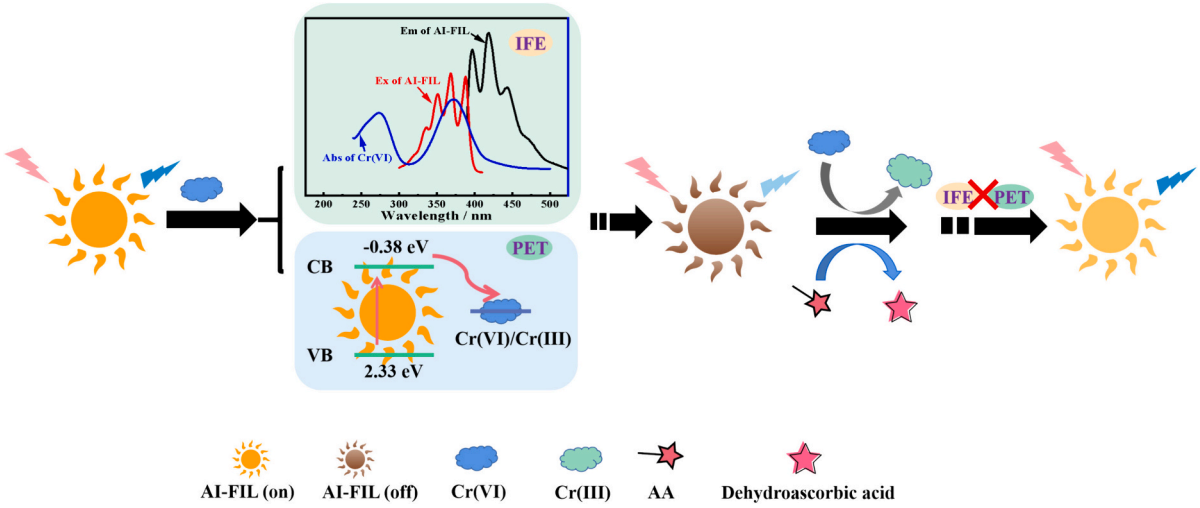

Scheme 1. Schematic diagram of the fluorescent assay based on AI-FIL for detecting Cr(VI) and AA.

were ground to powder, and then 0.5 g of powder or milk was mixed with K_2HPO_4 solution (0.1 M). After vortexing, ultrasound, and oscillation, the mixture was centrifuged for 5 min at 10,000 rpm to obtain supernatant. Finally, the supernatant was mixed with *n*-hexane and centrifuged for 5 min. After that, the supernatant was passed through a 0.45-μm filter membrane for further use. To investigate the fortified recovery of the newly developed fluoroprobe in environmental waters, the standard solutions of Cr(VI) were firstly introduced into the environmental waters. Then the mixed solutions with varying Cr(VI) concentrations were subjected to the pretreatment steps to obtain the spiked sample solutions. For the rice and milk samples, the standard solutions of Cr(VI) in the rice or milk samples were added to the K_2HPO_4 solutions (0.1 M), and then the mixed solutions were subjected to the following pretreatment processes to acquire the spiked sample solutions. After that, the spiked sample solutions (100 μL) were mixed with HAc-NaAc buffer (200 mM, pH 7.0, 800 μL) and AI-FIL (0.01 mg/mL, 100 μL), and the fluorescent emission spectra were recorded after a 5-min water-bath incubation.

For AA detection, the fresh fruits were selected as the real examples, and the samples were pretreated according to China's standard method (GB5009.86–2016). An amount of apple, kiwi, orange, strawberry, and tomato was first cleaned with ultrapure water and mashed to juice under room-temperature conditions. Aliquots of the resultant fresh juice samples were purified by 0.22-μm syringe filters, and the as-acquired supernatants were diluted 20-fold using Milli-Q ultrapure water before the test. To test the recoveries of the proposed fluoroprobe for AA, the standard solutions of AA were spiked into the resultant fresh juice samples, and then the mixed solutions were subjected to the following experiments according to the above-described pretreatment procedures to achieve the spiked sample solutions. Subsequently, the sample solution (100 μL) was thoroughly mixed with 900 μL of AI-FIL/Cr(VI). As described above, the fluorescent spectra of the mixed system were tested after a 40-min water-bath incubation.

2.5. Characterization and measurements.

^{1}H NMR and ^{13}C NMR analyses were carried out by a Bruker Avance NEO 600 MHz (Bruker, Germany). A Bruker Tensor II (Bruker, Germany) spectrometer was utilized to test the FT-IR spectra of as-prepared sample solutions. A Persee model TU-1901 spectrometer (Beijing, China) was used to acquire the spectral data on UV–vis absorption. The Agilent Cary5000 and Thermo Scientific ESCALAB 250Xi (CA, USA) were used to obtain and analyze the UV–vis-NIR DRS and XPS spectral information, respectively. Fluorescence emission spectra were achieved on an Edinburgh FS5 spectrofluorometer (London, England). The high performance liquid chromatography (HPLC) instrument (Shimadzu HPLC, LC-20AT, Japan), equipped with a diode-array detector (DAD), was used to detect AA in fresh fruits, and the detection parameters were referred to China's standard method (GB5009.86–2016), as described in electronic supplementary materials.

3. Results and discussion

3.1. Characterization of the AI-FIL

^{1}H NMR and ^{13}C NMR spectral information were used to characterize the as-synthesized AI-FIL. The corresponding data were summarized as follows: ^{1}H NMR (400 MHz, D_2O), δ 8.37 (s, 2H), 8.12 (s, 2H), 7.97 (dd, J = 11.1, 9.0 Hz, 8H), 7.60–7.49 (m, 8H), 7.28 (dd, J = 3.9, 1.7 Hz, 4H), 5.98 (s, 4H) (Fig. 1A); ^{13}C NMR (101 MHz, D_2O), δ 135.30, 130.63, 130.16, 130.01, 129.30, 127.81, 125.42, 123.46, 122.10, 121.89, 121.35, 44.69, 35.51 (Fig. 1B). As displayed in Fig. 1C, the sharp peak at ~3052 cm^{-1} belonged to the stretching vibration of aromatic C—H. Four strong signals at 1629, 1580, 1550, and 1445 cm^{-1} were assigned to the in-plane ring stretches. Two distinct peaks at ~1150 and 730 cm^{-1} belonged to the stretching vibration of C—N and the out-of-plane bending of aromatic C—H, respectively. The optical properties of AI-FIL were examined using UV–vis absorption and fluorescent spectra. AI-FIL displayed five absorption peaks at ~250, 333, 349, 367, and 387 nm, which were attributable to the $\pi \rightarrow \pi^*$ (Fig. 1D). Another absorption peak at ~215 nm was attributed to the absorption of imidazolium ring in the AI-FIL. For the excitation spectra, AI-FIL exhibited the four peaks at 335, 350, 370, and 390 nm. Three emission peaks were observed at 396, 418, and 443 nm when excited at 370 nm. As shown in the inset of Fig. 1D, the bright blue fluorescence of AI-FIL could be visually observed under a 365 nm UV lamp. To further investigate the fluorescent property of AI-FIL, the fluorescent emission peak was investigated under the different excitation wavelengths. The emission wavelength of AI-FIL remained nearly constant with increases in the excitation wavelength from 330 to 380 nm (Fig. S1), suggesting that it was excitation-independent. In addition, the FIs of AI-FIL displayed no obvious changes as the pH values increased up to 8.0 (Fig. S2), confirming that the as-synthesized AI-FIL possessed strong adaptability to solution pH. Subsequently, the steady-state kinetics and stability of AI-FIL were investigated in detail. It can be seen from Fig. S3A that the FIs of AI-FIL maintained 94.5% of its initial value even if irradiated for 12 h by using a 500 W Xe lamp, suggesting an excellent photostability of AI-FIL. Moreover, the FIs of AI-FIL remained 92.0% of its initial value after a 4-week storage at room temperature (Fig. S3B), demonstrating the satisfactory stability of AI-FIL.

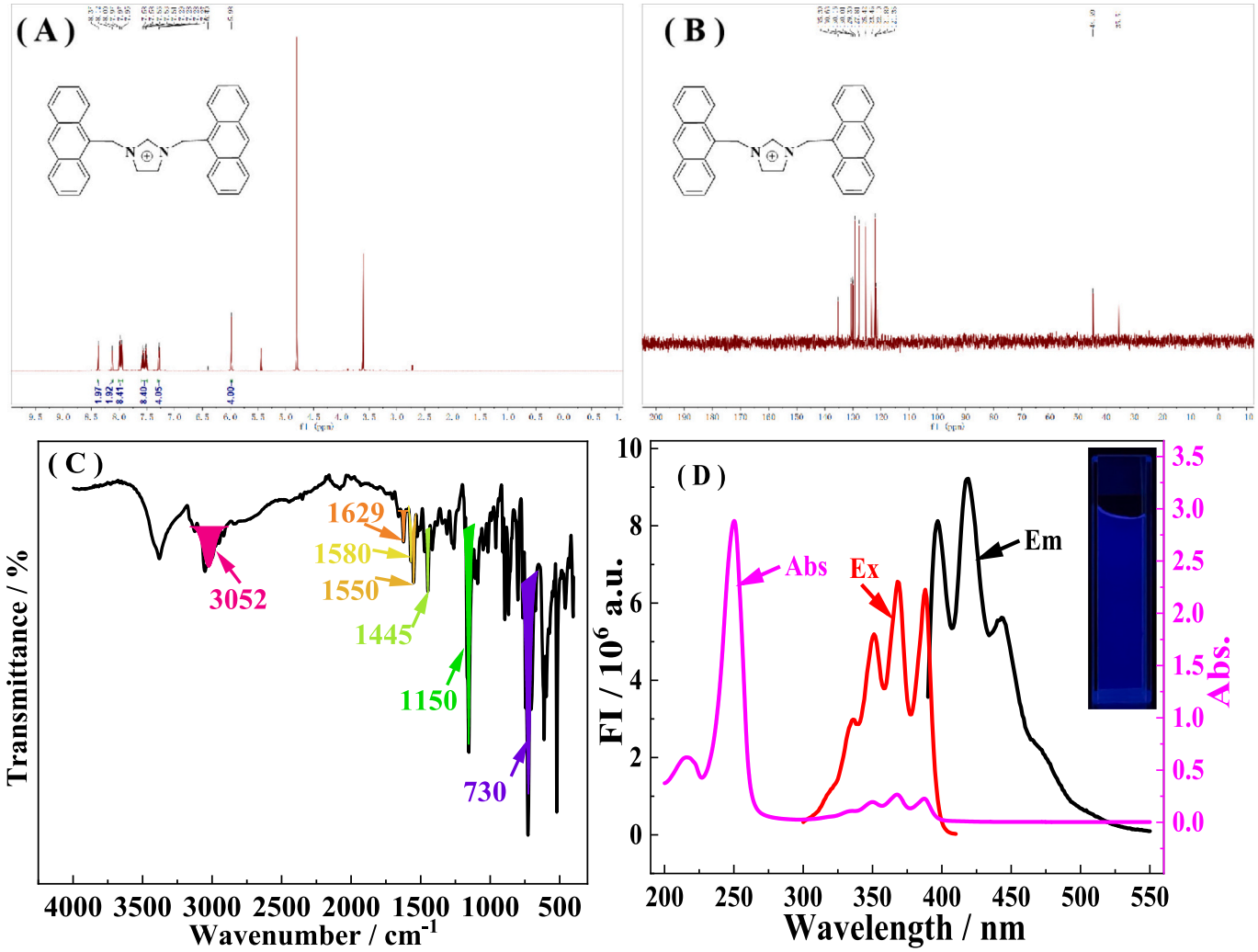

Fig. 1. ^{1}H NMR and ^{13}C NMR spectra of AI-FIL in D_2O; (C) FT-IR spectra of AI-FIL; (D) UV–vis absorption spectra of (Abs), fluorescent excitation (Ex) and fluorescent emission (Em) spectra of AI-FIL, Insert: photographs of AI-FIL under UV light at 365 nm.

3.2. Construction of the "on-off-on" fluoroprobe for Cr(VI) and AA detection

As shown in Fig. 2A, the FIs of AI-FIL significantly decreased upon the addition of Cr(VI), while they rapidly recovered following the addition of AA to the AI-FIL/Cr(VI) system. By contrast, the FIs of AI-FIL displayed no changes in the presence of AA alone. These findings demonstrate that the addition of Cr(VI) substantially decreased the FIs of AI-FIL, while AA restored the quenched FIs of AI-FIL/Cr(VI). The insert of Fig. 2A shows the images of different systems under a 365-nm UV lamp. As compared to AI-FIL, the blue fluorescence of AI-FIL turned to diminish with the addition of Cr(VI), while it was recovered to the original blue level in the presence of AA in the mixed system of AI-FIL/Cr (VI). However, the blue fluorescence of AI-FIL remained nearly unchanged despite the addition of AA. With regard to the UV–vis absorption, no obvious new peaks or shift of the maximum absorption was

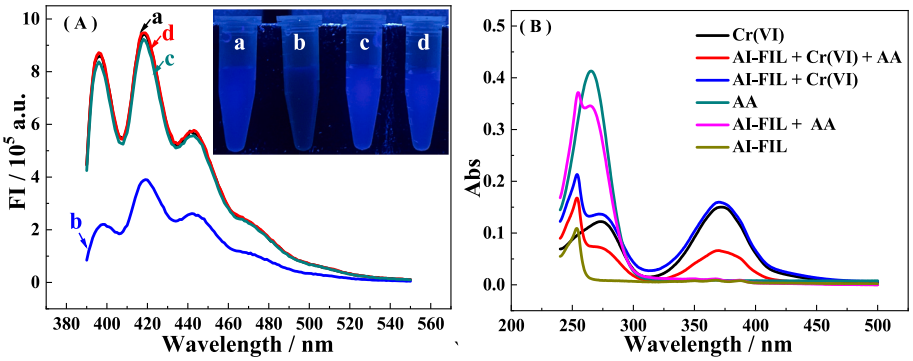

Fig. 2. (A) The fluorescence emission spectra of AI-FIL (a), AI-FIL + Cr(VI) (b), AI-FIL + Cr(VI) + AA (c) and AI-FIL + AA (d), Insert: the corresponding photographs under UV light at 365 nm; (B) UV–Vis absorption spectra of Cr(VI), AI-FIL, AA, AI-FIL + Cr(VI), AI-FIL + Cr(VI) + AA and AI-FIL + AA.

observed for the AI-FIL/Cr(VI) system in comparison to those of individual AI-FIL and Cr(VI) (Fig. 2B). In the AI-FIL/Cr(VI) and sole Cr(VI) systems, the characteristic peak intensity of Cr(VI) prominently decreased in the presence of AA when compared to that in the absence of AA, implying the significant reduction effect of AA on Cr(VI). To further confirm the occurrence of the above reduction phenomenon, the effects of AA at varying fortification concentrations on the UV–vis spectra were investigated in detail in the mixed system of AI-FIL/Cr(VI). As displayed in Fig. S4, the intensity of Cr(VI) around 360 nm reduced with the elevation of AA, demonstrating the reduction of Cr(VI) to Cr(III) (Zhang, Chen, Zou, Li, & Huang, 2018; Xu et al., 2019). These observations prove that the FIs of AI-FIL can be quenched by Cr(VI), while recovered by AA.

According to previous reports (Zhang, Fang, et al., 2018; Ma et al., 2017), fluorescence resonance energy transfer (FRET), IFE, or photo-induced electron transfer (PET) are the possible mechanisms to illustrate the underlying fluorescence-quenching process between Cr(VI) absorber and AI-FIL. As depicted in Fig. 3A, the UV–vis absorption spectrum of Cr(VI) was observed to be highly overlapped with the excitation spectrum of AI-FIL, hinting that the fluorescence quenching process might be related to the FRET or IFE process. To further investigate the underlying quenching mechanisms, the fluorescence lifetimes of AI-FIL were measured when fortified at varying Cr(VI) concentrations. The fluorescent decay curves of AI-FIL (a), AI-FIL/Cr(VI) (0.05 mM) (b), and AI-FIL/Cr(VI) (0.5 mM) (c) were well-fitted by a one-exponential function at the excitation wavelength of 350 nm (Fig. 3B). The average lifetimes of three systems were calculated to be 11.86, 11.67 and 10.50 ns, respectively. Interestingly, the fluorescence lifetimes of AI-FIL remained constant even when Cr(VI) was added, demonstrating that the quenched FIs of AI-FIL by Cr(VI) were related to the IFE process rather than the FRET process because those of AI-FIL would be remarkably changed during an efficient FRET process. To assess the role of IFE in fluorescence quenching, the observed quenched efficiency (E_q) and the corrected E_q after removing the IFE were figured out (Fig. S5 and Table S1). It can be seen that the corrected E_q was about 27.5%, and the quenched effect resulting from the IFE of Cr(VI) was ~46.3%. These data confirmed that the quenching process of AI-FIL by Cr(VI) primarily originated from IFE (Zhai, Wang, Yu, Wang, & Mao, 2014). To further reveal the mechanisms of the quenching process of Cr (VI) toward AI-FIL, DRS and valence band (VB) analyses from XPS were analyzed in detail (Fig. 3C). Based on the Kubelka-Munk function from DRS, the band gap of AI-FIL was computed to be 2.71 eV (Lin et al., 2018). The VB of AI-FIL was calculated to be 2.33 eV (Fig. 3D). According to the report by Wang and coworkers, the conduction band (CB) of AI-FIL was calculated to be −0.38 eV (Wang et al., 2017). As illustrated in Fig. S6, the redox potential for Cr(VI)/Cr(III) is 1.33 eV, which lies between the CB and VB of AI-FIL. As a result, it could be inferred that the photo-induced electron of AI-FIL under the 370 nm excitation wavelength transferred to the unfilled d-orbit of Cr(VI), leading to the fluorescence-quenching phenomenon. These observations demonstrate that Cr(VI) can quench the fluorescence of AL-FIL through a PET process. From the above discussion, we posit that the quenched FIs of AI-FIL by Cr(VI) belong to the joint IFE and PET processes. In stark contrast, the addition of AA led to prominently enhanced FIs of AI-FIL/Cr(VI) for the elimination of IFE and PET owing to the reduction of Cr(VI) to Cr(III) by AA (Zhang, Fang, et al., 2018; Xu et al., 2019).

3.3. Fluorescent detection of Cr(VI)

To gain excellent sensitivity of the AI-FIL based fluorescent detection, three main experimental parameters were rigorously optimized, including AI-FIL concentration, buffer pH, and reaction time between Cr (VI) with AI-FIL. When the concentration of AI-FIL was 0.01 mg/mL, the slope (k) of the E_q reached the maximum (Fig. S7), suggesting the most efficient quenching of AI-FIL by Cr(VI). Thus, the concentration of AI-FIL was set at 0.01 mg/mL to construct the fluorescent sensor. From Fig. 4A, the E_q increased as the pH increased to 7, then kept constant, further increasing the pH to 8. So, the optimal buffer pH value was set as 7. Fig. 4B shows the effects of reaction time between Cr(VI) and AI-FIL on the E_q values. The E_q elevated rapidly up to 55% within 1 min and remained nearly unchanged after 5 min, confirming that the Cr(VI)-triggered fluorescence-quenching process was rapid. Consequently, the appropriate reaction time was set at 5 min between Cr(VI) and AI-FIL.

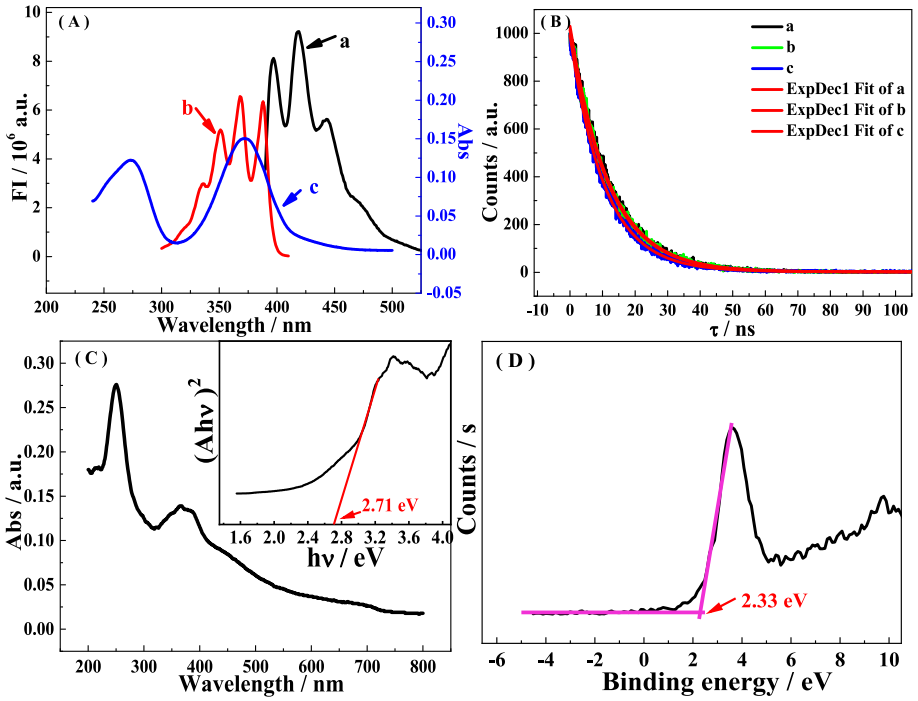

Fig. 3. (A) Fluorescent emission (a) and excitation (b) spectra of AI-FIL, and UV–Vis absorption spectra (c) of Cr(VI); (B) Fluorescence lifetime spectra of AI-FIL (a), AI-FIL/Cr(VI) (0.05 mM) (b) and AI-FIL/Cr(VI) (0.5 mM) (c); (C) UV–vis DRS spectra of AI-FIL, Insert: Kubelka-Munk plots converted from the UV–vis DRS spectra; (D) VB-XPS spectra of AI-FIL.

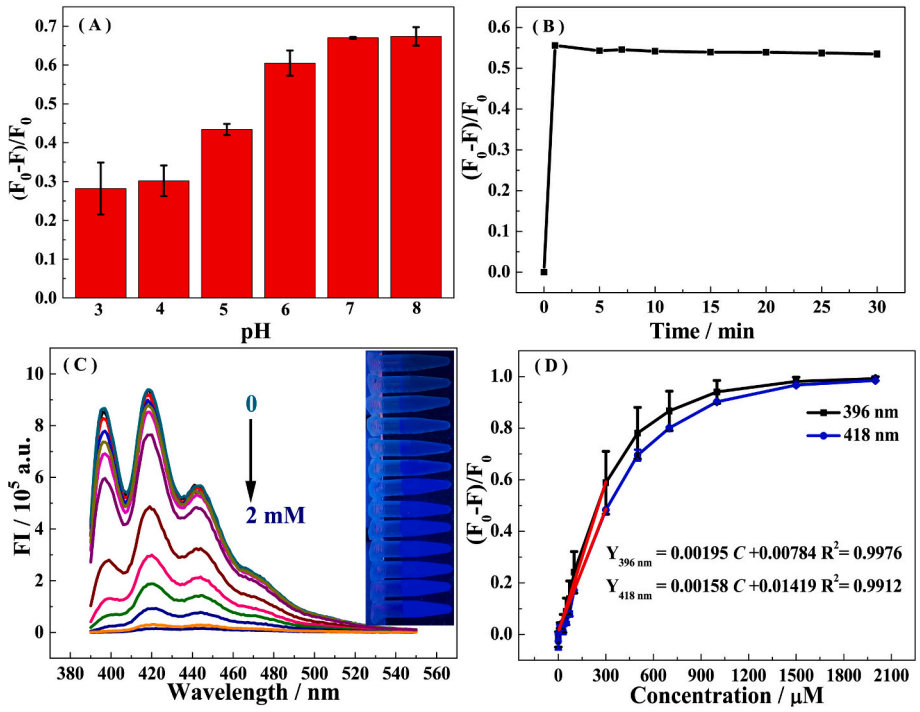

Fig. 4. Effect of buffer pH (A) and reaction time (B) between AI-FIL and Cr(VI); (C) The fluorescence emission spectra of AI-FIL with different concentrations of Cr (VI), Insert: the corresponding photographs under UV light at 365 nm; (D) The calibration plot of Cr(VI) determined by the fluorescent assay based on AI-FIL.

When fortified at the different concentrations of Cr(VI), the FIs of AI-FIL were investigated in detail to acquire the best fluorescent performance. When the Cr(VI) concentrations increased from 0 to 2 mM, the FIs of AI-FIL progressively decreased (Fig. 4C). Simultaneously, the color of AI-FIL gradually diminished from bright blue to dark blue as Cr(VI) was added to the system (insert of Fig. 4C). The E_q values significantly went up with increasing Cr(VI) concentrations with an excellent linear response from 0.03 to 300 μM (Fig. 4D). Based on S/N = 3 (N is estimated according to the standard deviation (SD) obtained from the blank sample, N=SD = 2.9×10^{-3}, $n = 10$), the limit of detection (LOD) of the as-constructed fluorescent detection was calculated to be 9 nM (Araujo, 2009). As listed in Table 1, the LOD (9 nM) by this fluorescence sensor is substantially lower than those (0.021–1.5 μM) by the fluorescence detection based on PNCQDs, S, N-CDs, Si-CQDs, MoS_2 QDs, SiQDs, SQDs, and g-C_3N_4 NSs (Duan et al., 2020; Gong et al., 2017; Hu, Zhang, Gan, Yin, & Fu, 2018; Ji et al., 2021; Liu et al., 2019; Rong et al., 2015; Tan et al., 2021; Xu et al., 2019), while it is comparable in contrast to those by N-CDs (5.0 nM) (Zhang et al., 2018) and GQDs (3.7 nM) (Huang et al., 2015). Significantly, the linear range (0.03–300 μM) of the AI-FIL based fluorescent detection for Cr(VI) is much wider than the previous methods (Duan et al., 2020; Gong et al., 2017; Hu et al., 2018; Ji et al., 2021; Liu et al., 2019; Rong et al., 2015; Tan et al., 2021; Xu et al., 2019) and is comparable with those by N-CDs and GQDs (Zhang et al., 2018; Huang et al., 2015). The threshold limit of Cr(VI) in groundwater stipulated by WHO was 1.9 μM, which suggested that the AI-FIL-based fluorescent detection was sensitive enough for trace-level Cr(VI) detection in environmental waters (Hu et al., 2018).

The high selectivity of the AI-FIL based fluorescence detection is vital in complex sample matrices. According to previous reports, the co-existing ions, such as Al^{3+}, Cu^{2+}, Zn^{2+}, Mg^{2+}, Ca^{2+}, Na^{+}, Ag^{+}, Co^{2+}, Ni^{2+}, Fe^{3+}, Fe^{2+}, Cr^{3+}, PO_4^{3-}, CO_3^{2-}, NO_3^{-}, and SO_4^{2-}, may interfere with accurate detection of Cr(VI) and were considered as the interferents (Huang et al., 2015; Zhang et al., 2018; Duan et al., 2020). In contrast to the E_q caused by Cr(VI), the E_q values caused by other interferents were negligible even if the concentrations of these interfering ions were fortified at 2-fold higher than the spiking level of Cr(VI) (Fig. S8). Only the

Table 1
Comparison of the fluorescent assay based on AI-FIL for detecting Cr(VI) and AA with other sensors.

Materials	Cr(VI)		AA		Ref.
	Linear range (μM)	LOD (μM)	Linear range (μM)	LOD (μM)	
PNCQDs	1.5–30	0.023	5–200	1.35	(Gong et al., 2017)
S, N-CDs	0.03–50	0.02114	1–1000	0.28	(Ji et al., 2021)
Si-CQDs	0.4–160	0.0336	1–80	0.0846	(Liu et al., 2019)
MoS_2 QDs	0.5–20	0.12	4–300	0.85	(Hu et al., 2018)
SiQDs	0.5–500	0.16	2–200	0.57	(Xu et al., 2019)
N-CDs	0.01–250	0.005	1–750	0.3	(Zhang et al., 2018)
SQDs	0.5–225	0.024	1–300	0.18	(Duan et al., 2020)
SQDs	10–120	0.36	20–500	1.21	(Tan et al., 2021)
g-C_3N_4 NSs	0.6–300	0.15	0.5–200	0.13	(Rong et al., 2015)
GQDs	0.05–500	0.0037	1–500	0.51	(Huang et al., 2015)
AI-FIL	0.03–300	0.009	1–1000	0.3	This work

Note: PNCQDs: phosphorus/nitrogen dual-doped carbon quantum dots; S, N-CDs: sulfur and nitrogen co-doped carbon dots; Si-CQDs: organosilane-functionalized carbon quantum dots; MoS_2 QDs: molybdenum disulfide quantum dots; SiQDs: water-dispersed silicon quantum dots; N-CDs: nitrogen-doped carbon dots; SQDs: sulfur quantum dots; g-C_3N_4 NSs: graphitic carbon nitride nanosheets; GQDs; graphene quantum dots.

UV–vis absorption spectrum of Cr(VI) was highly overlapped with the excitation spectrum of AI-FIL, demonstrating that co-existing metal ions, including Cu^{2+}, Co^{2+}, Ni^{2+}, Fe^{3+}, Fe^{2+}, Ag^{+}, and Cr^{3+}, could not quench the fluorescence of AI-FIL through the FRET and IFE processes (Fig. S9). Moreover, as shown in Fig. S6, the redox potentials of Fe(II)/Fe, Zn(II)/Zn, Cr(III)/Cr, Al(III)/Al, Mg(III)/Mg, Na(I)/Na, and Ca(II)/Ca didn't fall

within the range of CB and VB of AI-FIL, excluding the possibility of quenching the fluorescence of AI-FIL by the PET process. Although the redox potentials of Ag(I)/Ag, Fe(III)/Fe(II), Cu(II)/Cu, Ni(II)/Ni, and Co(II)/Co varied between CB and VB of AI-FIL, the E_q values of these related metal ions (Ag^+, Fe^{3+}, Cu^{2+}, Ni^{2+} and Co^{2+}) were all <0.1 as compared to that of Cr(VI) (0.7). These data provide compelling evidence that the fluorescence quenching of Cr(VI) toward AI-FIL is dominated by the IFE process, thereby yielding high selectivity (Zhang et al., 2018; Duan et al., 2020). The E_q values of the five-parallel tests toward Cr(VI) (300 μM) were recorded with the relative standard deviations (RSDs) of 2.4%, manifesting a satisfactory reproducibility of the AI-FIL based detection (Fig. S10).

To demonstrate the actual practicability of the present method, the AI-FIL-based fluorescent detection was used to detect Cr(VI) in real-world environmental waters. As generalized in Table 2 and Table 3, the concentrations of Cr(VI) in polished rice, brown rice, milk, river, lake and, tap waters were all not detectable, which evidenced that the Cr(VI) levels in the investigated food and water samples were all lower than the LOD of the newly developed fluorescent sensing detection. The spiking extraction recoveries for Cr(VI) spanned the range of 97.5–107.5% with RSDs <5.2% in food samples and 95.4–105.7% with RSDs <4.2% in water samples. Moreover, the results obtained by the fluorescent platform based on AI-FIL were in general accordance with the results according to China's standard method. The intra-day and inter-day precision, which was recorded as RSDs ($n = 3$), were obtained in the range of 1.3% to 4.2%. Therefore, we posit that the as-constructed AI-FIL-based fluorescent platform exhibits great potential for the conventional monitoring of trace-level Cr(VI) in foods and environmental waters.

3.4. Fluorescent detection of AA

For AA detection, the Cr(VI) concentration, buffer pH, and reaction time of AA with AI-FIL/Cr(VI) should be the main factors affecting the performance of the AI-FIL/Cr(VI) based fluorescent detection. Fig. 5A displays the effects of varying buffer pH on the recovered efficiencies for the AI-FIL/Cr(VI) + AA system. Clearly, the recovered fluorescent efficiencies for the AI-FIL/Cr(VI) + AA system increased first, then decreased, and finally reached a balanced level with the maximum value at pH 7.0. So, the buffer pH was set at 7.0 because alkaline conditions were not conducive to the AA-Cr(VI) redox occurrence (Yang et al., 2018). As elaborated in Fig. 5B, a monotonically declining trend was observed for the recovered efficiencies of the AI-FIL/Cr(VI) + AA system with the elevating Cr(VI) concentrations from 0.3 to 1.5 mM. Consequently, 0.3 mM of Cr(VI) was fortified for AA detection in the subsequent trials. With the prolongation of reaction time, the recovered fluorescent efficiency in the AI-FIL/Cr(VI) + AA system gradually increased and reached a stable level at 40 min (Fig. S11), implying that the Cr(VI)-AA redox attained the balance. Hence, 40 min was chosen as the appropriate reaction time in the following experiments.

Under optimized conditions, the fluorescence emission spectra of AI-FIL/Cr(VI) are shown in Fig. 5C at varying concentrations of AA. With the rising AA concentrations, the FIs of AI-FIL obviously increased, and the solution color varied from dark blue to bright blue. The recovered fluorescent efficiencies for the AI-FIL/Cr(VI) system were linearly elevated with the rising AA concentrations (1 μM to 1 mM) (Fig. 5D). Correspondingly, the LOD for AA was estimated to be 0.3 μM based on S/N = 3 (N=SD = 9.7×10^{-2}, $n = 10$). As listed in Table 1, the LOD (0.3 μM) of AA by the AI-FIL based fluorescent detection is comparable or even better than those (0.28–1.35 μM) by the previously reported approaches (Ji et al., 2021; Zhang et al., 2018; Gong et al., 2017; Hu et al., 2018; Hu et al., 2018; Tan et al., 2021; Huang et al., 2015). However, it is slightly higher than those by Si-CQDs, SQDs, and g-C_3N_4 NSs (0.084–0.18 μM) (Duan et al., 2020; Liu et al., 2019; Rong et al., 2015). In sharp contrast, the linear range (1–1000 μM) provided by the present method is much wider than the previous methods (Gong et al., 2017; Ji et al., 2021; Liu et al., 2019; Hu et al., 2018; Xu et al., 2019; Zhang et al., 2018; Duan et al., 2020; Tan et al., 2021; Rong et al., 2015; Huang et al., 2015). In contrast to the nanomaterials for fluorescent assay, such as CQDs, SiQDs, g-C_3N_4 NSs, MoS_2 QDs and SQDs, the synthetic steps of AI-FIL are relatively simple without requiring the complex purification process, including centrifugation and dialysis. Moreover, as a kind of "green" solvents, the fluoroprobe based on AI-FIL is more environmentally benign.

Moreover, the coexisting interferents, such as dopamine, L-cysteine, L-tryptophan, glycine, sucrose, glucose, DL-serine, sodium citrate dihydrate, and GSH, were used to investigate the selectivity for AA detection (Zhang et al., 2018; Xu et al., 2019; Duan et al., 2020). As shown in Fig. S12, these coexisting interferents had no or slight effects on the recovered efficiency of the as-developed fluorescence system. The characteristic absorption peak of Cr(VI) around 360 nm significantly declined in the presence of AA when compared to the coexisting reductive substances such as GSH, glucose, and dopamine (Fig. S13). The faint yellow of the Cr(VI) solution turned to colorless within AA, while the coexisting reductive substances didn't cause any color change (insert Fig. S13). These findings provide compelling evidence that the reducibility of AA is much stronger than those of the coexisting reductive substances, thus yielding satisfactory selectivity (Hathoot, Yousef,

Table 2
Analytical results of the fluorescent assay based on AI-FIL for detecting Cr(VI) in foods.

Samples	Added (mg/kg)	This method			SN/T2210–2021		
		Found (mg/kg)	Recovery (%)	RSDs (%)	Found (mg/kg)	Recovery (%)	RSDs (%)
Polished rice	0	ND.	/	/	ND.	/	/
	2	2.15	107.5	1.4	2.09	104.5	2.3
	5	4.89	97.8	3.8	5.12	102.4	4.5
	10	10.05	100.5	2.9	9.79	97.9	3.7
Brown rice	0	ND.	/	/	ND.	/	/
	2	1.98	99.0	3.1	2.13	106.5	1.9
	5	5.13	102.6	1.8	5.06	101.2	3.2
	10	9.75	97.5	2.7	10.04	100.4	4.8
Milk	0	ND.	/	/	ND.	/	/
	2	2.13	106.5	5.2	2.09	104.5	3.9
	5	5.23	104.6	4.3	5.07	101.4	5.2
	10	10.02	100.2	2.4	9.87	98.7	2.7

Note: The fortified "Found" concentration is equal to the actually detected value.
ND. represents the acronym of non-detectable.
RSDs (%) are achieved from the tests in triplicate.

Table 3
Analytical results of the fluorescent assay based on AI-FIL for detecting Cr(VI) in river water, lake water and tap water.

Samples	Added (μM)	This method					GB 7467–87		
		Found (μM)	Recovery (%)	RSDs (%)	Inter-day precision (RSD, %)	Intra-day precision (RSD, %)	Found (μM)	Recovery (%)	RSDs (%)
River water	0	ND.	/	/	/	/	ND.	/	/
	10	9.54	95.4	4.2	3.6	2.5	9.72	97.2	4.5
	50	50.39	100.8	2.6	2.1	1.3	51.28	102.6	3.8
	200	203.47	101.7	1.8	3.8	4.2	201.75	100.9	2.9
Lake water	0	ND.	/	/	/	/	ND.	/	/
	10	9.65	96.5	3.5	2.4	2.9	9.63	96.3	3.8
	50	51.76	103.5	2.1	1.7	3.2	52.97	105.9	2.5
	200	198.91	99.5	2.4	3.8	2.1	204.52	102.3	1.9
Tap water	0	ND.	/	/	/	/	ND.	/	/
	10	10.38	103.8	3.8	3.9	1.9	10.32	103.2	2.6
	50	52.87	105.7	2.9	1.4	2.8	51.43	102.9	2.3
	200	203.63	101.8	1.4	2.1	2.2	206.24	103.1	1.6

Note: The fortified "Found" concentration is equal to the actually detected value.
ND. represents the acronym of non-detectable.
RSDs (%) are achieved from the tests in triplicate.

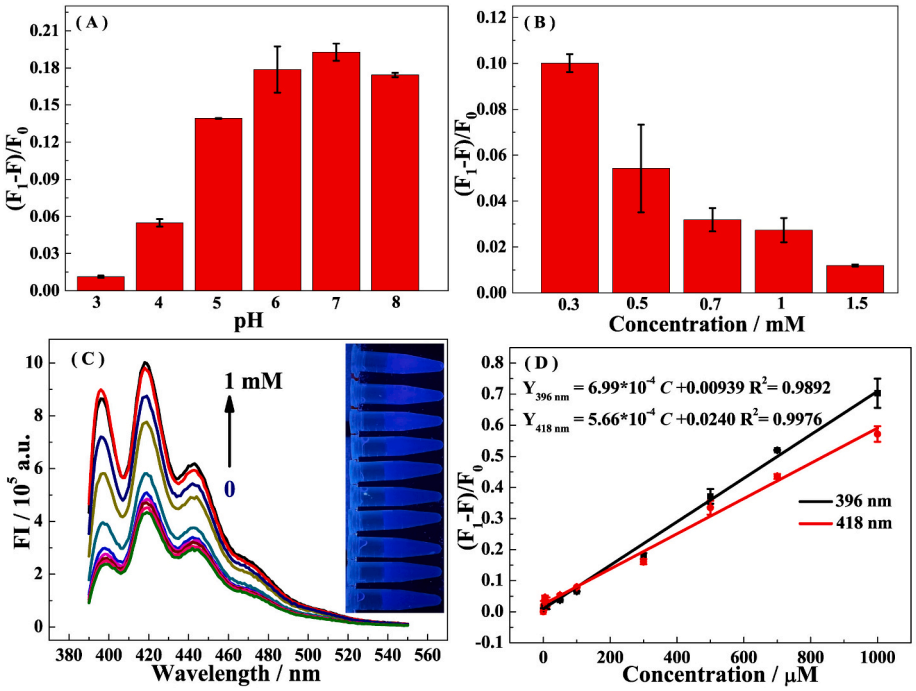

Fig. 5. Effect of the buffer pH (A) and concentration of Cr(VI) (B) for the determination of AA based on AI-FIL/Cr(VI); (C) The fluorescence emission spectra of AI-FIL/Cr(VI) with different concentrations of AA, insert: the corresponding photographs under UV light at 365 nm; (D) The calibration plot of $(F_1—F)/F_0$ versus the concentrations of AA based on AI-FIL/Cr(VI).

Shatla, & Abdel-Azzem, 2012). As a result, the AI-FIL/Cr(VI)-based sensing platform exhibits a superior anti-interfering effect for AA detection.

Fresh fruits were used to appraise the applicability of the as-developed fluorescence detection based on AI-FIL/Cr(VI) for AA detection. As generalized in Table 4, the concentrations of AA in apple, kiwi, orange, strawberry, and tomato were 4.96, 62.27, 25.64, 53.72, and 21.86 mg/100 g, respectively, which were almost consistent with the data detected by HPLC according to China standard method (GB5009.86–2016). Besides, the fortified recoveries for AA ranged from 93.2% to 106.7% with RSDs <4.6%, and the RSDs of intra-day and inter-day precision were in the range of 0.4–4.6%. These findings highlight that the as-developed fluorescent sensing platform is reliable and practical for AA detection in complex food matrices. To further verify the applicability of the fluorescent assay for Cr(VI) and AA detection, the commercial fruit juices (grape juice, lemon juice, and kiwi juice) were selected as real samples. As summarized in Table 5, the concentrations of AA in the grape, lemon and kiwi juices were determined to be 325.15, 967.38 and 731.63 μM, respectively, while Cr(VI) was not detectable, suggesting the concentrations of Cr(VI) were below its detection limit in these juices. The fortified recoveries ranged from 93.7% to 106.5% for Cr(VI) and 94.1% to 104.8% for AA with RSDs <5.1%, suggesting the feasibility of the fluorescent assay based on FILs in real samples.

Table 4
Analytical results of the fluorescent assay based on AI-FIL for detecting AA in foods.

Samples	Added (mg/100 g)	This method					HPLC (GB5009.86–2016)		
		Found (mg/100 g)	Recovery (%)	RSD (%)	Inter-day precision (RSD, %)	Intra-day precision (RSD, %)	Found (mg/100 g)	Recovery (%)	RSD (%)
Apple	0	4.96	/	4.6	3.2	2.6	4.83	/	3.6
	20	24.43	97.4	3.2	0.5	1.5	23.56	93.7	4.2
	100	105.31	100.4	2.6	1.0	2.1	106.06	101.2	3.6
	200	208.83	101.9	1.9	0.9	1.3	207.73	101.5	2.3
Kiwi	0	62.27	/	3.5	0.5	3.2	61.29	/	2.4
	20	80.90	93.2	3.3	4.3	0.8	80.52	96.2	2.9
	100	163.65	101.4	2.9	3.5	2.4	165.03	103.7	1.6
	200	269.18	103.5	1.2	3.1	1.8	266.07	102.4	3.5
Orange	0	25.64	/	3.8	3.6	1.9	24.93	/	2.8
	20	46.58	104.7	2.6	2.4	2.7	45.31	101.9	3.7
	100	127.92	102.3	3.7	3.7	1.2	128.88	104.0	4.2
	200	228.53	101.5	2.8	4.0	0.9	228.49	101.8	1.9
Strawberry	0	53.72	/	3.2	3.2	2.8	52.84	/	2.6
	20	74.58	104.3	2.9	3.3	1.7	72.47	98.2	3.9
	100	155.19	101.5	2.8	0.4	3.8	155.38	102.5	4.2
	200	259.65	103.0	1.6	4.6	2.6	257.46	102.3	3.1
Tomato	0	21.86	/	3.6	1.2	4.3	20.53	/	3.4
	20	43.20	106.7	3.2	2.8	3.2	40.76	101.2	2.6
	100	126.13	104.3	2.7	3.5	2.9	123.89	103.4	3.2
	200	230.68	104.4	2.3	2.1	1.8	226.40	102.9	2.3

Note: The fortified "Found" concentration is equal to the actually detected value.
RSDs (%) are achieved from the tests in triplicate.
HPLC represents high performance liquid chromatography.

Table 5
Analytical results of the fluorescent assay based on AI-FIL for detecting Cr(VI) and AA in commercial fruit juices.

Samples	Cr(VI)				AA			
	Added (μM)	Found (μM)	Recovery (%)	RSDs (%)	Added (μM)	Found (μM)	Recovery (%)	RSDs (%)
Grape juice	0	ND.	/	/	0	325.15	/	/
	10	10.65	106.5	3.6	200	532.53	103.7	5.1
	50	52.12	104.2	2.5	500	828.19	100.6	3.7
	200	187.46	93.7	1.9	1000	1273.20	94.8	2.4
Lemon juice	0	ND.	/	/	0	967.38	/	/
	10	9.75	97.5	1.3	200	1164.18	98.4	1.9
	50	48.37	96.7	2.3	500	1437.82	94.1	2.8
	200	196.8	98.4	3.9	1000	2015.35	104.8	3.4
Kiwi juice	0	ND.	/	/	0	731.63	/	/
	10	10.45	104.5	4.2	200	926.67	97.5	3.3
	50	47.89	95.8	3.1	500	1204.59	94.6	4.6
	200	207.63	103.8	2.6	1000	1750.36	101.9	1.8

***Note*:** The fortified "Found" concentration is equal to the actually detected value.
ND. represents the acronym of non-detectable.
RSDs (%) are achieved from the tests in triplicate.

4. Conclusions

As a proof-of-concept, an AI-FIL with superior fluorescent properties was successfully synthesized and used to construct a fluorescence-switch platform for Cr(VI) and AA detection. The fluorescence-quenching mechanisms resulted from the fact that the FIs of AI-FIL were distinctly decreased by Cr(VI) through the joint IFE and PET processes and restored because AA reduced Cr(VI) to Cr(III). Besides, the "on-off-on" fluorescent platform produced wider linear responses of 0.03–300 μM and 1–1000 μM with LODs of 9 nM and 0.3 μM for Cr(VI) and AA, respectively. To sum up, the newly developed "on-off-on" fluorescent platform based on AI-FIL displays several advantages, such as easy synthesis, excellent stability, environmental friendliness, good repeatability, satisfactory sensitivity, and high selectivity for the detection of Cr(VI) and AA. Moreover, it is feasible for both Cr(VI) and AA detection in real-world waters and foods with high accuracy and precision.

CRediT authorship contribution statement

He Mei: Methodology, Funding acquisition, Formal analysis. **Ping Xu:** Methodology, Investigation, Formal analysis. **Mengting Feng:** Formal analysis, Data curation. **Jianping Wang:** Investigation, Formal analysis, Data curation. **Chenxin Zhang:** Formal analysis, Data curation. **Haibin Chen:** Software, Data curation. **Huili Wang:** Methodology,

Investigation. **Junyi Guo:** Project administration, Methodology. **Xuedong Wang:** Supervision, Project administration. **Shugen Qu:** Supervision, Project administration.

Declaration of competing interest

The authors declare that they have no known competing financial interests or personal relationships that could have appeared to influence the work reported in this paper.

Data availability

Data will be made available on request.

Acknowledgments

This work was jointly supported by the National Science Foundation of China (22076134), Zhejiang Provincial Natural Science Foundation (LQ21B050004), Suzhou Key Project of Science and Technology (2022SS24), and South Zhejiang Institute of Radiation Medicine and Nuclear Technology (ZFY-2022-K-004).

Appendix A. Supplementary data

Supplementary data to this article can be found online at https://doi.org/10.1016/j.fochx.2024.101488.

References

Alizadeh, N., Ghasemi, F., Salimi, A., Hallaj, R., Fathi, F., & Soleimani, F. (2020). Polymer nanocomposite film for dual colorimetric and fluorescent ascorbic acid detection integrated single-cell bioimaging with droplet microfluidic platform. *Dyes and Pigments, 173*, Article 107875. https://doi.org/10.1016/j.dyepig.2019.107875

Araujo, P. (2009). Key aspects of analytical method validation and linearity evaluation. *Journal of Chromatography B, 877*, 2224–2234. https://doi.org/10.1016/j.jchromb.2008.09.030

Chen, B. H., Jiang, S. J., & Sahayam, A. C. (2020). Determination of Cr(VI) in rice using ion chromatography inductively coupled plasma mass spectrometry. *Food Chemistry, 24*, Article 126698. https://doi.org/10.1016/j.foodchem.2020.126698

Chen, K., Qing, W. X., Hu, W. P., Lu, M. H., Wang, Y., & Liu, X. H. (2019). On-off-on fluorescent carbon dots from waste tea: Their properties, antioxidant and selective detection of CrO_4^{2-}, Fe^{3+}, ascorbic acid and L-cysteine in real samples. *Spectrochim Acta Part A, 213*, 228–234. https://doi.org/10.1016/j.saa.2019.01.066

Deng, L., Huang, F., Zhang, A. M., Wang, T. T., Yang, M. H., Li, X. Q., & Chen, X. (2023). One-step ultrasonic preparation of stable bovine serum albumin-perovskite for fluorescence analysis of L-ascorbic acid and alkaline phosphatase. *Biosensors, 13*(8), 770. https://doi.org/10.3390/bios13080770

Duan, Y. X., Tan, J. S., Huang, Z. M., Deng, D. M., Liu, S. J., Wang, G., … L.. (2020). Facile synthesis of carboxymethyl cellulose sulfur quantum dots for live cell imaging and sensitive detection of Cr(VI) and ascorbic acid. *Carbohydrate Polymers, 249*, Article 116882. https://doi.org/10.1016/j.carbpol.2020.116882

Fu, C. L., Meng, L. J., Lu, Q. H., Fei, Z. F., & Dyson, P. J. (2008). A facile strategy for preparation of fluorescent SWNT complexes with high quantum yields based on ion exchange. *Advanced Functional Materials, 18*, 857–864. https://doi.org/10.1002/adfm.200701144

Gao, J. J., Xu, H., Hou, F. J., & Zhang, S. X. (2022). A "turn-on" DNA-scafolded silver-nanocluster probe for detection of tumor-related mRNA. *Analytical Sciences, 38*, 419–426. https://doi.org/10.1007/s44211-022-00063-0

Gong, X. J., Liu, Y., Yang, Z. H., Shuang, S. M., Zhang, Z. Y., & Dong, C. (2017). An "on-off-on" fluorescent nanoprobe for recognition of chromium(VI) and ascorbic acid based on phosphorus/nitrogen dual-doped carbon quantum dot. *Analytica Chimica Acta, 968*, 85–96. https://doi.org/10.1016/j.aca.2017.02.038

Greaves, T. L., & Drummond, C. J. (2008). Protic ionic liquids: Properties and applications. *Chemical Reviews, 108*, 206–237. https://doi.org/10.1021/cr068040u

Guo, X. J., Yang, F., Jing, L., Li, J., Li, Y. H., Ding, R., … Zhang,, X. M. (2022). In-situ generation of highly active and four-in-one $CoFe_2O_4/H_2$PPOP nanozyme: Mechanism and its application for fast colorimetric detection of Cr(VI). *Journal of Hazardous Materials, 431*, Article 128621. https://doi.org/10.1016/j.jhazmat.2022.128621

Hathoot, A. A., Yousef, U. S., Shatla, A. S., & Abdel-Azzem, M. (2012). Voltammetric simultaneous determination of glucose, ascorbic acid and dopamine on glassy carbon electrode modified by NiNPs@poly1,5-diaminonaphthalene. *Electrochimica Acta, 85*, 531–537. https://doi.org/10.1016/j.electacta.2012.08.063

Hu, L. Z., Zhang, Q., Gan, X. Y., Yin, W. L., & Fu, W. S. (2018). Switchable fluorescence of MoS_2 quantum dots: A multifunctional probe for sensing of chromium(VI), ascorbic acid, and alkaline phosphatase activity. *Analytical and Bioanalytical Chemistry, 410*, 7551–7557. https://doi.org/10.1007/s00216-018-1374-2

Huang, D. M., Qi, H. Y., Jing, J., Sami, R., Jing, T., Alsufyani, S. J., … N.. (2022). A continuously tunable full-color emission nitrogen-doped carbon dots and for ultrasensitive and highly selective detection of ascorbic acid. *Nanomaterials, 12*(4), 693. https://doi.org/10.3390/nano12040693

Huang, S., Qiu, H. N., Zhu, F. W., Lu, S. Y., & Xiao, Q. (2015). Graphene quantum dots as on-off-on fluorescent probes for chromium(VI) and ascorbic acid. *Microchimica Acta, 182*, 1723–1731. https://doi.org/10.1007/s00604-015-1508-6

Jayaraman, N., Palani, Y., RaoJonnalagadda, R., & Shanmugam, E. (2022). Covalently dual functionalized graphene oxide-based multiplex electrochemical sensor for hg (II) and Cr(VI) detection. *Sensors and Actuators B: Chemical, 367*, Article 132165. https://doi.org/10.1016/j.snb.2022.132165

Ji, Y. Y., Zou, X., Wang, W. J., Wang, T. F., Zhang, S. L., & Gong, Z. J. (2021). Co-doped S, N-carbon dots and its fluorescent film sensors for rapid detection of Cr (VI) and ascorbic acid. *Microchemical Journal, 167*, Article 106284. https://doi.org/10.1016/j.microc.2021.106284

Kebede, A., Tilachew, G., Chirfa, G., & Gure, A. (2022). Effervescence assisted dispersive liquid-liquid microextraction for spectrophotometric determination of chromium (VI) in water, tannery effluent, milk, and orange juice samples. *South African Journal of Chemistry, 76*, 127–133. https://doi.org/10.17159/0379-4350/2022/v76a18

Kim, G., Choi, D., & Kim, C. (2021). A benzothiazole-based fluorescence turn-on sensor for copper(II). *Journal of Fluorescence, 31*, 1203–1209. https://doi.org/10.1007/s10895-021-02752-x

Lin, T., Son, Z., Wu, Y., Chen, L., Wang, S., Fu, F., & Guo, L. (2018). Boron- and phenyl-codoped graphitic carbon nitride with greatly enhanced light responsive range for photocatalytic disinfection. *Journal of Hazardous Materials, 358*, 62–68. https://doi.org/10.1016/j.jhazmat.2018.06.053

Liu, Y. S., Li, W., Wu, P., Ma, C. H., Wu, X. Y., Luo, S., & Liu, S. X. (2019). Organosilane-functionalized carbon quantum dots and their applications to "on-off-on" fluorometric determination of chromate and ascorbic acid, and in white light-emitting devices. *Microchimica Acta, 186*, 516. https://doi.org/10.1007/s00604-019-3603-6

Long, C. C., Qing, T. P., Fu, Q., Jiang, Z. X., Xu, J., Zhang, P., & Feng, B. (2020). Low-temperature rapid synthesis of high-stable carbon dots and its application in biochemical sensing. *Dyes and Pigments, 175*, Article 108184. https://doi.org/10.1016/j.dyepig.2020.108184

Ma, Y. S., Cen, Y., Sohail, M., Xu, G. H., Wei, F. D., Shi, M. L., … Q.. (2017). A Ratiometric fluorescence universal platform based on N, cu Codoped carbon dots to detect metabolites participating in H_2O_2-generation reactions. *ACS Applied Materials & Interfaces, 9*, 33011–33019. https://doi.org/10.1021/acsami.7b10548

Rong, M. C., Lin, L. P., Song, X. H., Wang, Y. R., Zhong, Y. X., Yan, J. W., … X.. (2015). Fluorescence sensing of chromium (VI) and ascorbic acid using graphitic carbon nitride nanosheets as a fluorescent "switch". *Biosensors & Bioelectronics, 68*, 210–217. https://doi.org/10.1016/j.bios.2014.12.024

Tan, Q., An, X., Pan, S., Liu, H., & Hu, X. (2021). Hydrogen peroxide assisted synthesis of sulfur quantum dots for the detection of chromium (VI) and ascorbic acid. *Spectrochim Acta Part A, 247*, Article 119122. https://doi.org/10.1016/j.saa.2020.119122

Wang, M., Shi, R., Gao, M. J., Zhang, K. L., Deng, L. L., Fu, Q. F., … D.. (2020). Sensitivity fluorescent switching sensor for Cr(VI) and ascorbic acid detection based on orange peels-derived carbon dots modified with EDTA. *Food Chemistry, 318*, Article 126506. https://doi.org/10.1016/j.foodchem.2020.126506

Wang, S., Lu, Q., Yan, X., Yang, M. M., Ye, R. F., Du, D., & Lin, Y. H. (2017). "On-off-on" fluorescence sensor based on g-C_3N_4 nanosheets for selective and sequential detection of ag^+ and S^{2-}. *Talanta, 168*, 168–173. https://doi.org/10.1016/j.talanta.2017.03.004

Xu, W., Yu, L. S., Xu, H. F., Zhang, S. Q., Xu, W., Lin, L., & Zhu, X. (2019). Water-dispersed silicon quantum dots for on-off-on fluorometric determination of chromium(VI) and ascorbic acid. *Microchimica Acta, 186*, 673. https://doi.org/10.1007/s00604-019-3751-8

Yang, H., He, L., Long, L. W., Li, H. X., Pan, S., Liu, H., & Hu, X. L. (2018). Fluorescent carbon dots synthesized by microwave-assisted pyrolysis for chromium(VI) and ascorbic acid sensing and logic gate operation. *Spectrochim Acta Part A, 205*, 12–20. https://doi.org/10.1016/j.saa.2018.07.015

Zhai, W. Y., Wang, C. X., Yu, P., Wang, Y. X., & Mao, L. Q. (2014). Single-layer MnO_2 nanosheets suppressed fluorescence of 7-hydroxycoumarin: Mechanistic study and application for sensitive sensing of ascorbic acid in vivo. *Analytical Chemistry, 86*, 12206–12213. https://doi.org/10.1021/ac503215z

Zhang, Q. Q., Chen, B. B., Zou, H. Y., Li, Y. F., & Huang, C. Z. (2018). Inner filter with carbon quantum dots: A selective sensing platform for detection of hematin in human red cells. *Biosensors & Bioelectronics, 100*, 148–154. https://doi.org/10.1016/j.bios.2017.08.049

Zhang, Y. H., Fang, X., Zhao, H., & Li, Z. X. (2018). A highly sensitive and selective detection of Cr(VI) and ascorbic acid based on nitrogen-doped carbon dots. *Talanta, 181*, 318–325. https://doi.org/10.1016/j.talanta.2018.01.027

Zhang, Y. Q., Liu, J. X., Wu, X. H., Tao, W. Q., & Li, Z. (2020). Ultrasensitive detection of Cr(VI) ($Cr_2O_7^{2-}/CrO_4^{2-}$) ions in water environment with a fluorescent sensor based on metal-organic frameworks combined with sulfur quantum dots. *Analytica Chimica Acta, 1131*, 68–79. https://doi.org/10.1016/j.aca.2020.07.026